Green technology to help calculate subsurface geothermal zones and temperatures before drilling

G. Stove[1*], O. Delgado[1], D. Limmer[1] and L. Lawrence[1] outline research and development for subsurface geothermal heat identification in various sites onshore UK.

Abstract

Geothermal energy is simply the natural heat that exists within our planet. The potential for harnessing electricity and heat from geothermal energy has long been recognised in Iceland, Hungary and New Zealand (Shere, 2013). Geothermal power has considerable potential for growth. The amount of heat within 10,000 m of the earth's surface is estimated to contain 50,000 times more energy than all oil and gas resources worldwide (Shere, 2013).

The most challenging aspect of geothermal exploration is the quantification of subsurface temperature conditions. Actual temperature conditions often remain very uncertain as it is difficult to remotely measure through several hundreds of metres of solid rock. Only drilling through the rock layers will give information on the existing subsurface temperature. As drilling is very expensive (€1million to €15million), any low-cost pre-drilling temperature estimation can bring in huge added value. Electromagnetic (EM) technology that Doel & Stove (2016) has been developing and experimenting aims to find subsurface sources of geothermal heat prior to drilling.

Through empirical field experimentation, EM technology would appear to non-invasively and digitally provide a temperature proxy measurement of the subsurface without physical drilling the Earth's crust. Although not everything is known about the technology's capabilities, EM technology shows strong promise. Key aspects of the technology have been field tested, including depth and capacity to identify water. Even at this early stage of development, EM technology merits further investigation to enable efficient and optimal exploration of the natural resources useful for geothermal energy generation.

Introduction

We are currently in the 'Geothermal decade' and by 2030 the sector will be 13 times bigger (EGEC 2020). To achieve the Paris Agreement temperature goal, countries aim to reach global peaking of greenhouse gas emissions as soon as possible to achieve a climate-neutral world by 2050. Reducing the reliance on high-carbon fossil fuels for generation of electricity and heating by transitioning to natural, zero-carbon geothermal solutions will help towards achieving UN Sustainable Development Goal 13 (climate action). All of the oil majors have started to ramp-up their activities in geothermal energy.

As part of the Energy Transition, we have been researching the use of electromagnetic (EM) radiowaves to endeavour to measure temperature in the Earth's crust. Given that radiowaves are good at identifying conductive water layers, the hypothesis is that radiowaves should be able to pick out the conductivity associated with hot rock layers in the ground associated with deep aquifers.

This paper outlines Adrok's self-funded, inhouse research and development for subsurface geothermal heat identification in various sites onshore UK. There are two different types of geothermal energy; low enthalpy (low temperature) resources that can provide warm water for direct applications, and high enthalpy (high temperature) resources that can yield hot water that is capable of driving turbines and generating electricity (Gillespie et al., 2013).

Within the sites selected in NE England (Figure 1), there are two different geological settings that have a large impact on the geothermal scenarios that may be encountered. The first geological setting in Eastgate is situated directly above the Weardale Granite, which drilling has pinpointed at depths of 390 m and 270 m, respectively (Manning et al, 2007). The Weardale Granite is expected to be a strong source of heat in the area, with post-drilling logging at Eastgate showing a temperature of 46.2°C at 995 m (10-15°C higher than the UK average). Significant volumes of hot saline water were also encountered during drilling at Eastgate, particularly at 410 m depth (PB Power, 2005). The second geological setting in Science Central, in Newcastle, is situated within successions of carboniferous limestones and sandstones. This means that the geothermal setting is likely to be a deep aquifer related to heat transfer from the many granite batholiths in NE England. Drilling at Science Central has confirmed a high geothermal gradient of 39°C/km (13°C/km higher than the UK average), with a potential reservoir in the Fell Sandstone at 1418 m deep (Younger, 2016). Unfortunately, our virtual boreholes ('V-Bore' is the name given to Adrok's electronic subsurface measurements) at Science Central locations have an end depth of 1368 m, so we cannot analyse the Fell Sandstone as a potential hot sedimentary aquifer. We can make assumptions on the geological settings based on the BGS geology maps.

In addition, and more conventionally, radioactive granites were measured in United Downs, Cornwall, SW England for

[1] Adrok
[*] Corresponding author, E-mail: gstove@adrokgroup.com
DOI: 10.3997/1365-2397.fb2022090

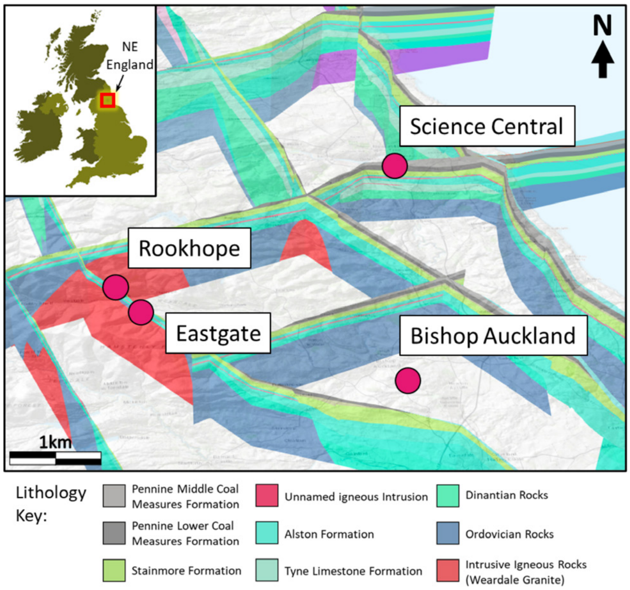

Figure 1 Location map and geology of NE England sites.

subsurface temperature changes (prior to drilling). More speculatively, an undrilled site in NE Scotland where suspected old red sandstones would show similar high temperatures to analogous North Sea settings (Gillespie et al., 2013) was also included in this research programme.

Method

The Atomic Dielectric Resonance (ADR) technology is based on the principle that different materials will reflect and absorb electromagnetic radiation (radio waves) at specific frequencies and energy levels. The ADR geophysical system transmits a pulse of electromagnetic energy containing a multispectral, patented (Stove, 2005) wave packet that resonates and reacts with the sub-surface materials. The reflections from the subsurface are recorded as a time domain trace and provide information about the location and composition of the materials encountered.

The ADR signal generator produces a pulse of electromagnetic energy (frequencies typically range between 1MHz to 70MHz) that is fed to the antenna and is transmitted into the ground. Once the signal has been sent to the transmitting antenna a signal is sent to the receiving control unit to synchronise collection of the subsurface reflected data, which is collected through the receiving antenna and then digitized. The transmitted pulse is depicted in Figure 3 where we also show the power spectrum (Stove & Doel, 2015). It is not the usual localized pulse with a single centre frequency but a more complicated waveform. The higher frequency components allow accurate localization at shallow depths, but attenuate rapidly in the ground, while the lowest frequency component around 3Mhz can penetrate much deeper. We thus combine the advantage of high spatial resolution at high frequencies with the advantage of greater depth penetration at low frequencies at the expense of requiring more sophisticated analysis (Doel et al., 2014).

When rocks of different compositions and textures have been exposed to ADR wave packets, a range of energy and frequency responses are detectable by suitable receivers. The recorded data describe how rocks and minerals, including hydrocarbons, interact with the electromagnetic radiation as it passes through them and pinpoints their composition. The technology calculates the dielectric permittivity of the subsurface as well as characterizing the nature of the rock types based on analysis of both the spectroscopic and resonant energy responses.

ADR is a time domain electromagnetic (TDEM) method but differs significantly from methods such as inductive polarization (IP) and resistivity methods. Those methods employ much lower frequencies and do not involve propagating waves but rely on measuring currents and polarizations induced by (relatively) slowly varying electric or magnetic fields. ADR on the other hand uses propagating wave packets and derives subsurface properties from the changes in spectral content and energy measured in the reflections. As such the data analysis resembles seismic methods more than the usual TDEM inversion techniques. However, ADR waves are electromagnetic which are governed by different physics than seismic pressure waves.

Adrok has developed ray tracing and finite-difference time-domain (FDTD) simulation software for numerical simulation of the ADR wave propagation through various subsurface materials (Doel & Stove, 2016). Simulated scans are used for preliminary feasibility studies and for experimental design of specific field scans using ground models based on known geology and/or borehole data if available.

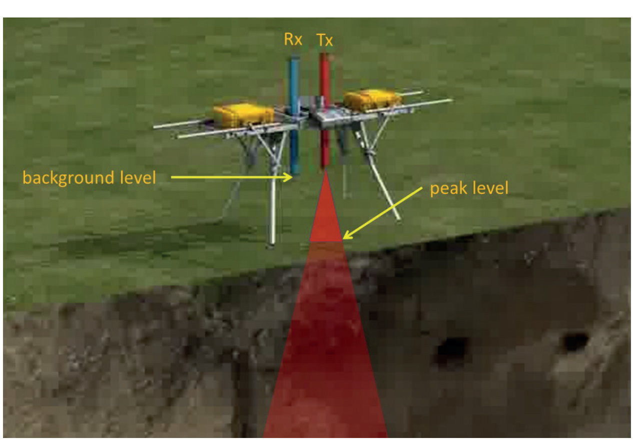

Figure 2 The electromagnetic pulse emitted by Tx enters the ground and subsurface reflections are recorded at the receiver Rx. Noise level is defined as the ratio of the background noise at the receiver and the peak signal when entering the ground.

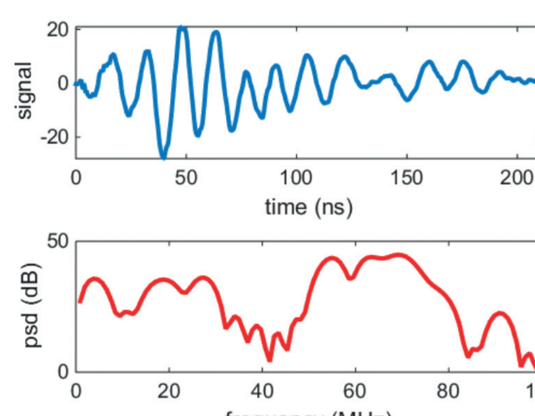

Figure 3 Example of an ADR EM wave packet in the time domain and its power spectral density.

Wave propagation model

Adrok has implemented a one-dimensional time-domain finite difference simulation of Maxwell's equations in a medium described by dielectric $\epsilon r(x)$, static conductivity $\sigma(x)$ and a Debye polarization model (Debye, 1929) with relaxation time τ to account for frequency-dependent losses (Doel & Stove, 2018). The model is similar to the one described in (Ciarletti et al., 2003), except we added a polarization component. Material properties are assumed to be constant in time but can depend on location. The model is summarized by the following system of partial differential equations (PDE):

$$\epsilon_0 \frac{\partial^2 E(t,x)}{\partial t^2} + \sigma(x)\frac{\partial E(t,x)}{\partial t} + \frac{\partial^2 P(t,x)}{\partial t^2} - \frac{1}{\mu_0}\frac{\partial^2 E(t,x)}{\partial x^2} = 0,$$

$$\tau(x)\frac{\partial P(t,x)}{\partial t} + P(t,x) = \epsilon_0(\epsilon_r(x) - 1))E(t,x)$$

with E the electrical field, P the polarization, $\epsilon 0 = 8.85 \times 10^{-12}$ F/m and $\mu 0 = 4\pi \times 10^{-7}$ H/m.

The equations are discretized with a fourth order finite difference approximation for the spatial derivatives and a leap-frog method for the time stepping (Ascher, 2008). At the simulation boundaries we use perfectly matched layers (Berenger, 1994). A spatial grid spacing of 10 cm and a time step of 0.15ns was used and found to be accurate enough for frequencies up to 100MHz. The size of the absorbing boundaries was 400 m on the top and 200 m on the bottom.

This model permits the simulation of Stare (or stationary antenna) scans, where transmitter and receiver are at (almost) the same position on the surface. During Wide Angled Reflection and Refraction (WARR) scans we measure returns with transmitter and receiver at increasing separations. For this a two-dimensional simulation is required. Due to the small grid spacing necessary and the long simulation times to capture deep reflections a FDTD simulator would require very large computational resources. For this reason we used a ray tracing method instead. A ray emitted from the transmitter is intersected with a boundary from a layered earth model, and the ray is split into a transmitted and reflected ray using standard geometric optics methods. These two rays then hit other boundaries and are split again, leading to an exponential growth of the number of rays which we cull by tracking the amplitude attenuation due to reflection coefficients and propagation losses and dropping rays that are attenuated more than 60dB. After all rays are computed the received returns on a line on the surface are rendered by propagating the output of the transmitter through all rays and applying frequency-dependent attenuation as obtained from the FDTD model. We also add a direct ground wave component.

The emitted pulse of the modelled system was obtained experimentally by measuring the propagating pulse measured in air as a time domain trace, and its waveform is used as the initial value condition of the PDE given above. The pulse is about 200ns long and contains frequency components from 2 to 70MHz with significant peaks at 3, 20, 30, and 65MHz (Doel et al., 2014). Noise levels (background and internal) were measured experimentally to be about 1% of the peak value of the amplitude at a distance of 1 m and are added to the simulated (noise-free)

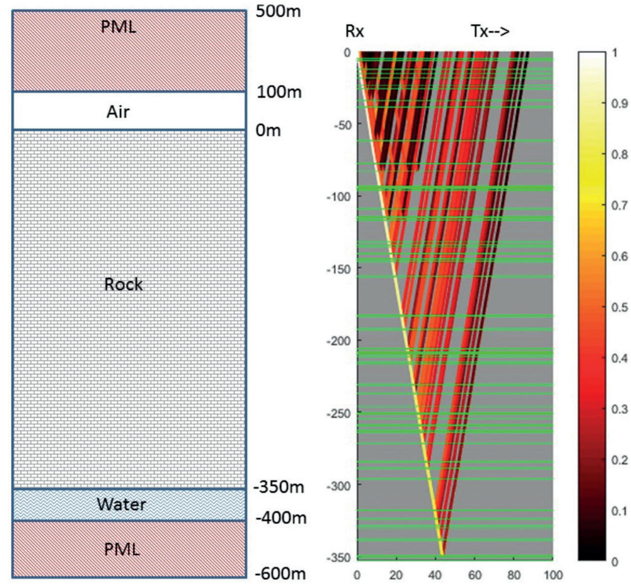

Figure 4 On left: Example of a simulation domain consisting of air, rock, and a reflecting water layer. The domain is padded on both sides with perfectly matched layers to eliminate unphysical reflections from the domain boundaries. On the right: a single ray propagating in the domain. Horizontal green lines divide regions with slightly different dielectric. The ray, computed from receiver (Rx) to transmitter (Tx) using time-invariance, splits at each intersection. Amplitude decreases in accordance with the reflection coefficients and propagation losses and is indicated in colour, with 1 the initial relative amplitude. Data is collected at the surface on a grid of locations. A total of 5000 rays are computed at various angles and added.

measurements as Gaussian noise of the same amplitude. The experimentally found noise spectrum was found to be Gaussian. In normal operation mode the receiver collects 500 traces which are stacked for noise reduction. Maximum acquisition rate for 20µs long traces is 10,000 traces per minute. The sampling rate is 2.5GHz.

Results indicate that with the modelled equipment a water layer (using a dielectric constant value of 81) can be detected quickly at a depth of 350 m through resistive host rock such as permafrost by detecting the arrival time of the reflection using a correlation analysis of a stare scan and a phase-based velocity spectrum analysis of a WARR scan over a 100 m line (Figure 4). Small irregularities in dielectric of about 0.25 are beneficial for the interpretation but if these fluctuations become very large multiples interfere with dielectric estimation. Under the constraint of a one-day experiment (including a WARR scan) and limitations on the scan rate, maximum exploration depth was estimated at 600 m (Doel & Stove, 2018). Results from this specific scenario may be applicable to exploration in other highly resistive Earth-based materials such as granite, igneous rocks, and certain types of coal (Reynolds, 1998).

The depth of penetration of the transmitted pulsed EM wave packets can be tuned to different transmission frequencies and energies (and two-way travel times) to suit different distance scales of propagation through solid objects. Maxwell's equations govern electromagnetic phenomena in vacuum only. To model propagation in materials such as the earth a specific model of the electrical properties of the earth has to be created and then coupled to the Maxwell equations (Doel et al. 2014, Doel & Stove, 2016). Such models are phenomenological and usually have

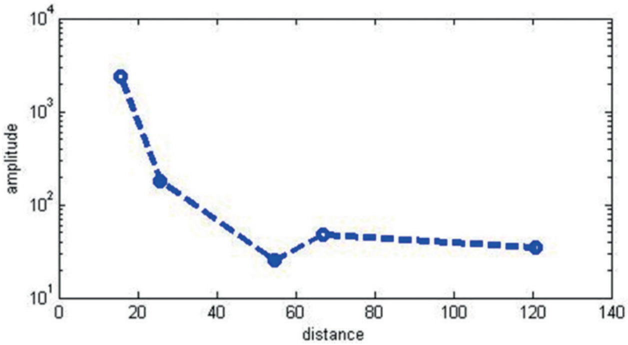

Figure 5 Empirically determined strength of ADR signal penetration, showing signal strength, lessens with depth but does not reach zero. There is a measured increase from 55 to 65 m which still needs to be explained through further research.

several parameters that are difficult to measure in-situ. For deep penetration applications for subsurface natural resource mapping at the geological scale, a wavelength of 30 m tends to be used (as this is the wavelength that has empirically been measured to penetrate deeper in field and modelling experimentations). Though this limits the resolution, i.e., the minimal separation at which distinct reflectors can be imaged to about 30 m, well-separated discrete reflectors can be localized more accurately using phase information, limited theoretically only by sampling rate and noise levels.

The measured signal strength versus distance (as demonstrated in the paper by Doel et al., 2014) is shown in Figure 5 below:

Depth is measured from time and velocity by ray tracing and Normal Move Out (NMO) computations, similar to the methods used in the seismic industry (Stove et al., 2018).

Results

Adrok has developed a suite of statistical signal processing techniques to assist information extraction of the resonant signal returns obtained from their ADR sensors following transmission through soil, sediment and rock layers and reception by a matched bistatic ADR receiver.

The resulting processed data suite is a specific set of logs which display signal frequency and energy returns. To evaluate mathematically and statistically the exact nature of the signal oscillations through time and space (depth), Adrok has developed a series of precise measures, of which E-Gamma shows the most promising correlation to ground-truthing. E-Gamma is commonly used in image processing and is sometimes called 'modulation', see for example Mather and Koch (2011).

The E-Gamma results showed the most promising correlation to ground-truthing (by way of drill log results comparison) across all of the drill locations (Figure 6, for example).

Eastgate 2 was scanned as the authors had access to drill log information at this location from the publication by PB Power et al. (2005). When the three Stare scans at Eastgate 2 (EG2) sites' E-Gamma's are averaged, all three low E-Gamma anomalies are identified. The first low E-Gamma anomaly at a depth of 440-490 m can only be seen when we increase the range of the E-Gamma charts, as it has much lower values than the average for EG2. The key correlation between E-Gamma and the downhole observed temperature is where the temperature jumps up from 20°C to above 25°C around 400 m, where we are getting the significant E-Gamma responses.

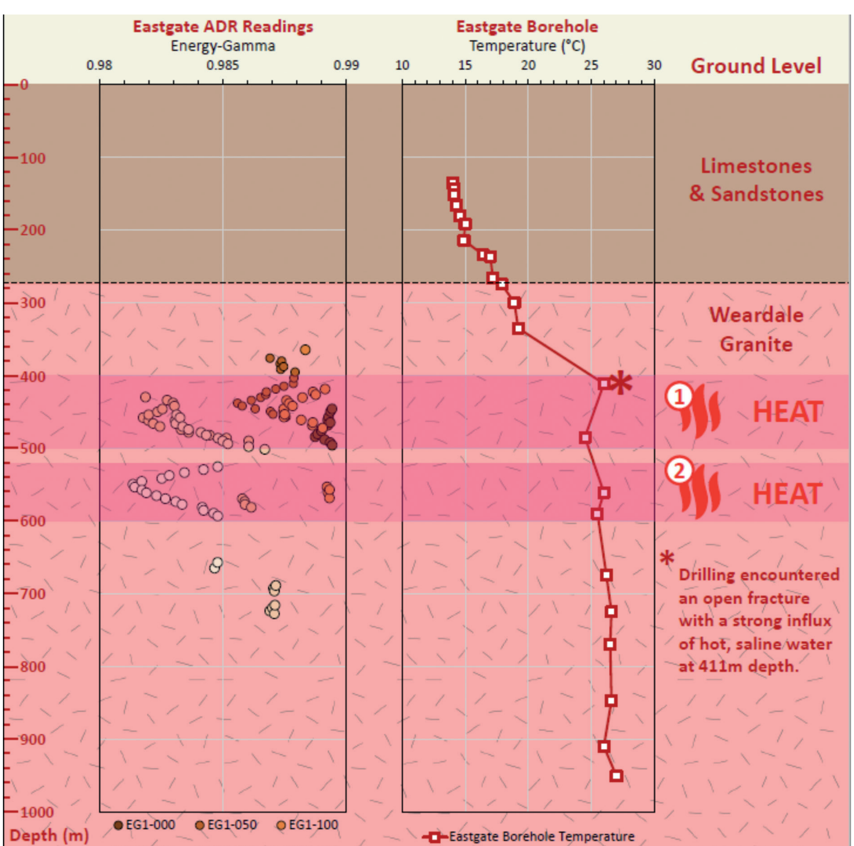

Figure 6 Eastgate 2 site E-gamma readings in NE England shown on left-hand graph versus observed temperature at Eastgate 2 site physical drillhole in NE England right-graph alongside lithology log on right-hand-side (observed temperature data from PB Power et al 2005). EG1-000 to EG2-100 signify the site names where ADR readings were collected.

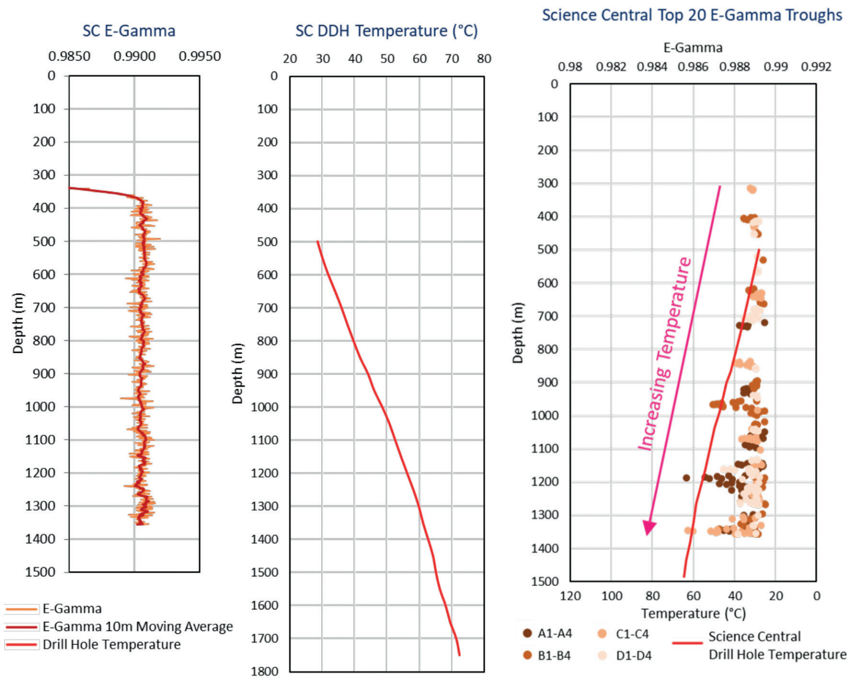

Figure 7 Science Central geothermal site (NE England) showing E-Gamma (left graph), Drill Hole Temperature (middle graph, data from Younger et al, 2016) and the 20 E-Gamma troughs (right graph).

The other two E-Gamma anomalies are located at depths of 530-610 m & 640-690 m. The remainder of the E-Gamma has a few minor E-Gamma troughs but they are all less significant than the three shallower anomalies.

The method of identifying E-Gamma troughs as temperature anomalies appears to be good for targeting hot zones due to the high contrast in temperature with adjacent units. There is a good observational relationship that would be worth researching further to work out why this is the case. However, this method is not effective at identifying geothermal gradients, in particular, the enhanced geothermal gradient of 39°C/km that is known at Science Central. However, we caution that we would still need to explore whether the E-Gamma technique is picking out temperature or water saturation effects (or a mixture of both effects).

Changes in subsurface temperature will affect conductivity and permittivity, as discussed by Kummerow and Raab (2015), which will affect the radar returns. Due to the diffuse nature of the temperature gradients, we will not see sharp reflections as in conventional subsurface imaging with GPR or seismic but more complicated effects. Initial analysis of the data set suggested the modulation Mather and Koch (2011), widely used in remote sensing, as a candidate parameter to correlate with temperature. Variations in subsurface geology will also affect results and we have disentangled these effects from temperature effects through machine learning (Doel et al. 2021).

A new method has been developed in order to pinpoint the 'hottest' horizons with more precision and accuracy. The top 20 'troughs' or low values of E-Gamma for each V-Bore (below the beam saturation) have been selected and plotted together with depth in order to gain greater insights into the areas that yield the most heat. So, when the top 20 E-Gamma troughs for all 16 Science Central V-Bores are plotted, a new trend is seen that hints towards an increasing temperature with depth that is not seen from the raw E-Gamma plots. In Science Central, the abundance of E-Gamma troughs increases with depth. The troughs also become more enhanced (lower E-Gamma values) with depth, suggesting that there is indeed a linear geothermal gradient. The patterns from the top 20 E-Gamma troughs correlate well with the Science Central borehole temperature log, suggesting that there is an enhanced geothermal gradient of ~39°C/km (13°C/km higher than the UK average). The E-Gamma shows an inverse relationship with temperature, with a 10°C increase in temperature correlating with a 0.001 decrease in E-Gamma. The E-Gamma troughs indicate temperatures of ~60°C at 1350 m depth in Science Central. (Figure 7). Again, these may just be speculative correlations without justification. Further research would be required to prove these correlations.

In Cornwall, we present results from 2017 United Downs data sets (ahead of drilling that was completed in summer 2021). The drill results have yet to be made public, but we present our results as a prediction prior to drilling (Figure 8).

In NE Scotland, our hypothesis is that the old Dalradian Sandstones will contain heat (based on our prior knowledge of oil industry drilled holes in the North Sea). The preliminary fieldwork was conducted at two sites close to the coast near Elgin. The results show temperature change at depth (Figure 9). Based on experience, there are good indications of a low enthalpy geothermal system in the form of a hot sedimentary aquifer in Units 4 and 5 450-650 m. This is a high-confidence geothermal target due to the combination of a significant direct water indication (DWI) target and a high temperature anomaly from a different method of data processing using machine learning which we are currently developing. A full description of the machine learning approach falls outside the scope of this paper. This method is applicable when temperature logs as well as ADR scans are available at a sufficiently large number of locations and is based on training a neural network

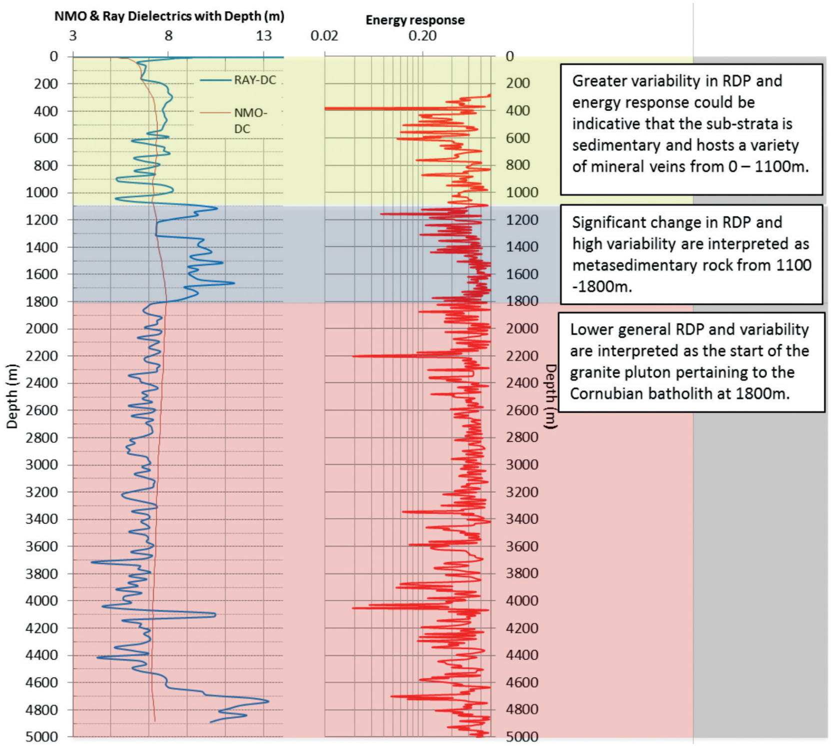

Figure 8 Virtual Borehole logs at the United Downs site in Cornwall (England) showing Dielectrics (right graph) and E-Gamma (left graph), with interpretation of the main lithological changes. No drill hole for comparison. Speculative virtual borehole experiment prior to drilling.

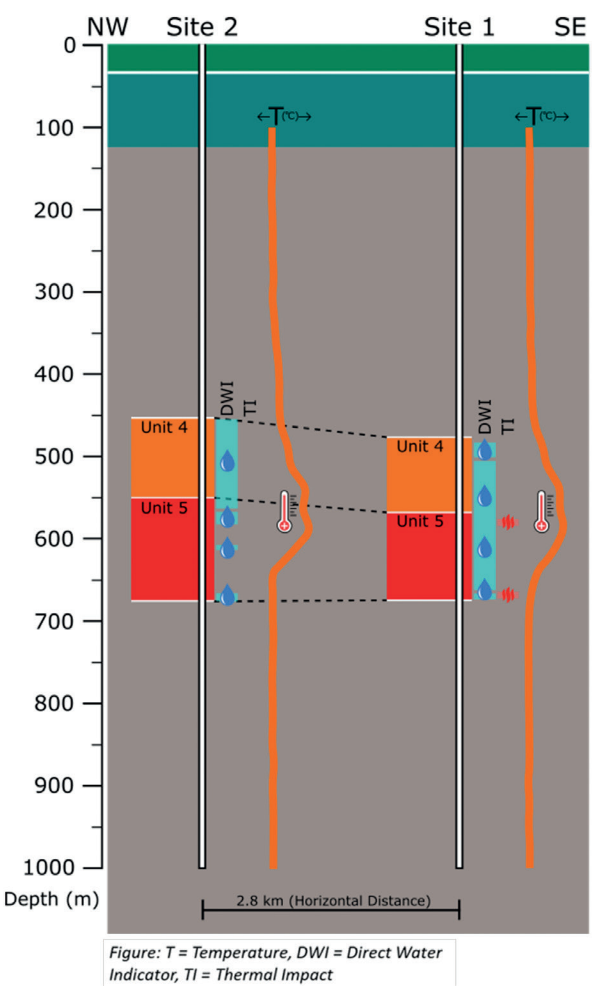

Figure 9 Virtual Borehole temperature measurement near Elgin (NE Scotland) showing discernible lithology units, water finds and temperature profiles. No drill hole for comparison. Speculative virtual borehole experiment prior to drilling.

to reconstruct the temperature profiles from the ADR data and temperature logs. Details of this method applied to enhanced oil recovery methods using steam injection at up to 40 sites are described in Doel et al. (2021). For the cases at hand, we have only a small amount of temperature logs for training (three) which is why we do not stress the approach in this paper. The economic implications for these findings are that a confirmed geothermal resource near Elgin could provide a home-grown, low-carbon and green alternative to Scotland's heat and energy generation.

Conclusions

The interpreted results show that the technology can identify the highest temperatures below the ground and measure their depths with reasonable accuracies. Moreover, the technology demonstrates repeatability in measurements. The field measurements show encouraging potential for the technology to be applied as a pre-drilling tool in onshore geothermal plays around the world, given the ease of survey deployment and low environmental footprint.

We acknowledge that this technique is still in its infancy and requires more work to explain the relationships. Is this method picking up changes in temperature or changes in water or a mixture of both? We do not (and cannot) claim to fully understand why it works at this stage, but the case studies we have worked on have shown consistent matches to reality.

It would be interesting to apply this methodology to other electromagnetic (EM) subsurface measurement methods such as resistivity surveys which should also be able to see a relation between resistivity and temperature which perhaps could be disentangled from the geological features. We would probably need to visit an oilfield to obtain fuller subsurface measurements.

References

Ascher, U. [2008]. Numerical methods for evolutionary differential equations: SIAM.

Berenger, J. [1994]. A perfectly matched layer for the absorption of electromagnetic waves: *Journal of Computational Physics*, 114, 185-200.

Ciarletti, V., Martinat, B., Reineix, A., Berthelier, J.J. and Ney, R. [2003]. Numerical simulation of the operation of the gpr experiment on netlander: *Journal of Geophysical Research*, 108.

Debye, P. [1929]. Polar molecules: Chemical Catalogue Company.

Doel, van den, K., Jansen, J., Robinson, M., Stove, G.C. and Stove, G.D.C. [2014]. Ground penetrating abilities of broadband pulsed radar in the 1-70MHz range, proc. SEG, Denver.

Doel, van den, K. and Stove, G. [2016]. Modeling and Simulation of a Deeply Penetrating Low Frequency Subsurface Radar System, proc. EAGE, Vienna.

Doel, van den, K. and Stove, G.D.C. [2018]. Modelling and Simulation of Low Frequency Subsurface Radar Imaging in Permafrost: *Computer Science and Information Technology*, **6**(3), 40-45.

Doel, van den, K. and Stove, G. [2018]. Modeling and Simulation of Low Frequency Subsurface Radar Imaging in Permafrost: *Computer Science and Information Technology*, **6**(3), 40-45.

Doel, van den, K., Stove, G.D.C., Robinson, M.J. and Stove, G.C. [2021]. Monitoring subsurface temperature from radar scans using machine learning with applications to EOR using thermal injection, Conference Proceedings, IOR 2021, Apr 2021, Volume 2021, p.1-10, European Association of Geoscientists & Engineers (EAGE).

European Geothermal Energy Council (EGEC, 2020) https://www.egec.org/geothermal-decade-2/.

Gillespie, M.R., Crane, E.J. and Barron, H.F. [2013]. Study into the potential for deep geothermal energy in Scotland. www.scotland.gov.uk/Resource/0043/00437996. pdf: AECOM Energy/The Scottish Government.

Kummerow, J. and Raab, S. [2015]. Temperature Dependence of Electrical Resistivity Part II: A New Experimental Set-up to Study Fluid-saturated Rocks. *Energy Procedia*, 76, 247-255.

Mather, P.M. and Koch, M. [2011]. Computer Processing of Remotely-Sensed Images. John Wiley and Sons, Ltd., London.

Manning, D.A.C., Younger, P.L., Smith, F.W., Jones, J.M., Dufton, D.J. and Diskin, S. [2007].

Deep geothermal exploration well at Eastgate, Weardale, UK: a novel exploration concept for low-enthalpy resources. *Journal of the Geological Society*, 164, 371-382.

PB Power & University of Newcastle [2005]. Eastgate Geothermal Exploration Borehole, Final Report. British Geological Survey, NY93NW97.

Reynolds, J. M. [1998]. An introduction to Applied and Environmental Geophysics: John Wiley & Sons.

Shere, J. [2013]. Renewable: The World-Changing Power of Alternative Energy. St Martin's Press: New York, p. 201.

Stove, G.C. [2005]. Radar Apparatus for Imaging and/or Spectrometric Analysis and Methods of Performing Imaging and/or Spectrometric Analysis of a Substance for Dimensional Measurement, Identification and Precision Radar Mapping, USA Patent No.: 6864826, Edinburgh, GB: US Patent Office.

Stove, G.D.C. and van den Doel, K. [2015]. Large depth exploration using pulsed radar. In: ASEG-PESA Technical Program Expanded Abstracts 2015, Perth. 1-4.

Stove G. October 2018. Extending the Reach of Radio Waves for Subsurface Water Detection, Canadian Society of Exploration Geophysicists (CSEG).

Stove, G.D.C., Stove, G.C., and Robinson, M. [2018]. New method for monitoring steam injection for Enhanced Oil Recovery (EOR) and for finding sources of geothermal heat. Australasian Exploration Geoscience Conference 2018 (AEGC), Sydney.

Younger, P.L., Manning, D.A.C., Millward, D., Busby, J.P., Charles, R., Jones, C. and Gluyas, J.G. [2016]. Geothermal exploration in the Fell Sandstone Formation (Mississippian) beneath the city centre of Newcastle upon Tyne, UK. *Quarterly Journal of Engineering Geology and Hydrogeology*, **49**(4), pp.350-363.